 doi:10.20944/preprints201801.0124.v1

Article

Damping ratio in carbon fiber reinforced epoxy filament-wound composites using Hilbert transform

Enzo Costamilan[1], Alexandre M. Löw[1], Marcos D. F. Awruch[2], José Humberto S. Almeida Jr.[3]*, Sandro C. Amico[4], Herbert M. Gomesa[2]

[1] Mechanical Engineering Department, UFRGS, Av. Osvaldo Aranha 99, 90135-190 Porto Alegre, RS, Brazil
[2] Mechanical Engineering Department, UFSM, Av. Roraima, 1000, 97105-900 Santa Maria, RS, Brazil
[3] Composite Materials Department, Leibniz-Institut für Polymerforschung Dresden e.V., Hohe Straße 6, 01069 Dresden, Germany
[4] PPGE3M, Federal University of Rio Grande do Sul, Av. Bento Gonçalves 9500, 91501-970 Porto Alegre, RS, Brazil

* Correspondence: humberto@ipfdd.de; Tel.: +49 351 4658 1423

Abstract: The aim of this work is to evaluate damping ratio (ζ) of unidirectional carbon fiber-reinforced epoxy laminates using an experimental approach, which is then input into a finite element numerical model. The logarithmic decrement and the envelope techniques were calculated using Hilbert transform. Flat unidirectional laminates were manufactured by dry-filament winding and evaluated under dynamic free vibration tests (longitudinally and transverse fiber-oriented specimens). Post-processing and data analysis were carried out with a dedicated code which used a band-pass filter to isolate the first fundamental frequency from the other modes of vibration and from noise in the acquired signal, and then applied the Hilbert transform to estimate the vibration envelope and adjust an exponential curve to it to evaluate structural damping ratio. The experimental results for modal frequencies were compared to numerical predictions from a fitted finite element model.

Keywords: Hilbert Transform; damping ratio; vibration; finite element modeling; filament winding

1. Introduction

Damping is a key feature to characterize the dynamic behavior of fiber-reinforced composites regarding minimization of resonant vibrations. Different sources of energy dissipation include viscoelastic character of the matrix, fiber arrangement, damping due to fiber/matrix interface, damage, viscoelastic and thermoelastic damping [1]. The control of vibrations and noise in structures can be achieved by using active or passive damping systems, for instance [2,3]. Anyway, for dynamic loadings, damping ratio measurements are essential for performance control and structural safety.

The dynamic nature of damping in orthotropic materials is more complex than in isotropic ones due to the combined influence of several parameters, such as degree of orthotropy, fiber orientation, manufacturing method, boundary conditions as well as the vibrating mode on damping and stiffness distributions [4]. There are many methods available for structural damping evaluation related to modal analysis in mechanical structures, namely half-power bandwidth method, logarithmic decrement, rational fraction polynomial, random decrement, subspace stochastic identification (SSI) and fractional energy loss per cycle [5]. Many of them are also applied to evaluate elastic properties and those based on structural vibrations or acoustic measurement are commonly used in composite materials [6].

Damping of a composite system can be evaluated, for instance, based on the damping ratio (ζ) or the loss factor (η), which is used in *hysteretic* damping models. In those, the vibration decay of an

Preprints (www.preprints.org) | NOT PEER-REVIEWED | Posted: 15 January 2018 doi:10.20944/preprints201801.0124.v1

excited specimen is followed to characterize the damping behavior. The frequency amplitudes are measured by accelerometers and calculated using a digital method, for instance [7].

Hanselka and Hoffman [8] evaluated unidirectional glass/epoxy composites applying the resonance technique and found maximum damping when the fibers were oriented at 15º and 45º. Dubenets and Yakovenko [9] determined the effective complex moduli and vibration decrements of fiber-reinforced viscoelastic composites based on the finite element method. Wei and Kukureka [10] used acoustic energy emission and resonance techniques to measure the elastic properties of glass/epoxy composites and evaluated damping in terms of internal friction energy using either logarithmic decrement in free vibration or half power bandwidth, obtaining similar damping values from both techniques. Fenza et al. [11] minimized damping ratio data dispersion, and the associated uncertainties, by applying logarithmic decrement and Hilbert transform to obtain the free vibration decaying envelopes in the time domain for composites at different temperatures. Lavanya et al. [12] evaluated damping behavior of glass/epoxy composites using the half-power bandwidth technique and concluded that the highest damping was found for fibers oriented at 60°.

In this context, the aim of this paper is to investigate damping ratio of carbon fiber reinforced epoxy filament wound laminates, in the longitudinal and transverse fiber direction, by applying the logarithmic decrement technique and Hilbert transform. Experiments were carried out and post-processing of the obtained data is performed by a finite element (FE) model.

2. Logarithmic decrement applied to damping evaluation

Materials and Methods should be described with sufficient details to allow others to replicate and build on published results. Please note that publication of your manuscript implicates that you must make all materials, data, computer code, and protocols associated with the publication available to readers. Please disclose at the submission stage any restrictions on the availability of materials or information. New methods and protocols should be described in detail while well-established methods can be briefly described and appropriately cited.

Research manuscripts reporting large datasets that are deposited in a publicly available database should specify where the data have been deposited and provide the relevant accession numbers. If the accession numbers have not yet been obtained at the time of submission, please state that they will be provided during review. They must be provided prior to publication.

Logarithmic decrement method enables evaluation of damping ratio for a particular composite system based on free vibration responses. For a theoretical SDOF (single degree of freedom) mass-spring-damper system, the logarithmic decrement (δ) can be calculated as the natural logarithm of the ratio between any two successive positive peak amplitudes of the free vibration response [13]. The free vibration response of an underdamped SDOF system may be described by:

$$x(t) = X_0 e^{-\zeta\omega_d t}\sin(\omega_d t + \theta) \quad (1)$$

where X_0 is the initial magnitude, θ is the phase shift and ω_d the damped natural frequency.

Considering any two successive peaks separated by n oscillation cycles, the ratio between these amplitudes is:

$$\frac{x_n}{x_0} = e^{\frac{-2\pi n\zeta}{\sqrt{1-\zeta^2}}} \quad (2)$$

and the logarithmic decrement is calculated as:

$$\delta = \ln\left(\frac{x_1}{x_2}\right) = \frac{2\pi\zeta}{\sqrt{1-\zeta^2}} \quad (3)$$

Expanding the expression above for n cycles between the peaks:

$$\delta = \frac{1}{n}\ln\left(\frac{x_0}{x_{0+n}}\right) \quad (4)$$

Therefore, damping ratio may be obtained from the logarithmic decrement by:

$$\zeta = \frac{\delta}{\sqrt{(2\pi)^2 + \delta^2}} \quad (5)$$

And, for small values of ζ (<0.1), the following approximation is used:

$$\delta \cong 2\pi\zeta \quad (6)$$

Preprints (www.preprints.org) | NOT PEER-REVIEWED | Posted: 15 January 2018 doi:10.20944/preprints201801.0124.v1

3. Application of Hilbert transform for envelope and damping evaluations

This section may be divided by subheadings. It should provide a concise and precise description of the experimental results, their interpretation as well as the experimental conclusions that can be drawn.

Free response vibration signals generally present one (or more) resonance frequencies, also called carrier signal, and another signal corresponding to damping, that modulates (decreasingly) the carrier signal. Thus, the information about damping comes merged with the carrier wave, making the analysis more difficult.

The determination of an envelope is an efficient way to work around this problem [14], which is usually done via hardware, with special purpose circuit boards called envelope detectors, or digitally, applying the Hilbert transform [15]. This research focuses on the latter approach, and consists in applying a convolution operation ($\otimes$) which keeps function mappings at the same domains (i.e. time domain). The Hilbert transform pair is defined as:

$$x_h(t) = H\{x(t)\} = \frac{1}{n}x(t) \otimes \frac{1}{t} \quad (7)$$

$$x(t) = H^{-1}\{x_h(t)\} = -\frac{1}{\pi}x_h(t) \otimes \frac{1}{t} \quad (8)$$

Since both functions are described in the time domain, it is possible to combine them as:

$$z(t) = x(t) + jx_h(t) \quad (9)$$

The $z(t)$ function is called the analytical signal of $x(t)$, and is a complex signal in which its imaginary part is the Hilbert transform of $x(t)$. Equation (9) can then be rewritten as:

$$z(t) = A(t)e^{j\theta(t)} \quad (10)$$

where:

$$A(t) = \sqrt{[x^2(t) + {x_h}^2(t)]} \quad (11)$$

$$\theta(t) = \tan^{-1}\left[\frac{x_h(t)}{x(t)}\right] = 2\pi f_0 t \quad (12)$$

In Equations (11-12), $A(t)$ is the envelope of the response signal $x(t)$, and $\theta(t)$ is the instantaneous phase of $x(t)$. The Hilbert transform, $A(t)$, can be used as a tool for demodulating a constant amplitude and frequency sinusoidal signal, using an inverse exponential decay function to yield the modulated signal (the envelope), where the vibration decrement is due to damping.

4. Experimental procedure

Carbon fiber reinforced epoxy towpreg (Toray T700-12K-50C and UF3369 resin) from TCR Composites was used to produce flat laminates using a rectangular stainless steel mandrel (327 × 228 × 12 mm3) and a filament winding system from MFTech coupled with a KUKA robot KR 140 L100. The towpregs were wound onto the mandrel and a shrink tape was used to help consolidation. The laminates were cured by hot compression under 6 ton for 4 h at 130 °C, reaching a final fiber volume fraction of ≈72%. Unidirectional 4- and 8-layer laminates were produced and cut following longitudinal and transverse directions, yielding [0]4, [90]4, [0]8 and [90]8 specimens. However, the [90]4 laminates could not be used because they were not stiff enough to produce reliable results.

Table 1 shows the material properties of the carbon/epoxy composite system and Table 2 presents the four specimens of each family fixed into a clamped-free condition and tested in free vibration response. The data acquisition system was composed of two types of sensors: an Analog Devices ADXL 213 accelerometer, weighing 0.3 g, with 970 mV/g nominal sensitivity, nonlinearity of 0.5% of the full scale and ±1.2 g measurement range; and a Micro-Epsilon OptoNCDT 1300 laser vibrometer sensor, with 10 μm resolution, ± 10 mm dynamic measurement range and 250 mV/mm sensitivity. The latter one is considered a nonintrusive method since no mass is added to the clamped-free structure. The experimental set-up is shown in Figure 1.

The measurements were programmed in Keysight Agilent VEE 7.5 using a Measurement Computing 1208FS A/D board, with 12 bits, 8 input analog channels and a measurement range of ±10 V. The test was repeated 10 times for each specimen and post-processing of acquired data was performed in Matlab 2012, which consisted in selecting the free vibrating part of the signal, filtering its frequency contents around fundamental frequency of the beam followed by evaluating the Hilbert

Preprints (www.preprints.org) | NOT PEER-REVIEWED | Posted: 15 January 2018 doi:10.20944/preprints201801.0124.v1

transform to detect the envelope of dynamic response, fitting the exponential curve into that envelope, and then finally calculating the damping ratio. Some options available in the Matlab Signal Processing Toolbox for curve fitting were tested and the 'peaks' option was found to result in lower uncertainty.

Table 1. Representative properties of the carbon/epoxy 1-D laminate [16].

Property	Description	Value
E1 (GPa)	Longitudinal elastic modulus	129.3
E2 = E3 (GPa)	Transverse elastic modulus	9.11
ν12 = ν13	Poisson's ratio in planes 1-2/1-3	0.32
ν23	Poisson's ratio in plane 2-3	0.35
G12 = G13 (GPa)	Shear moduli	5.44
G23 (GPa)	Transverse shear modulus in plane 2-3	2.10
Xt (MPa)	Longitudinal tensile strength	1409.9
Yt (MPa)	Transverse tensile strength	42.5
Xc (MPa)	Longitudinal compressive strength	−740.0
Yc (MPa)	Transverse compressive strength	−140.3
Spl (MPa)	In-plane shear strength	68.9

Table 2. Specimens used in the free vibration tests.

Configuration	Length [mm]	Width [mm]	Thickness [mm]
$[0]_8$	234	28.0	3.00
$[0]_8$	203	28.0	3.00
$[0]_8$	195	29.0	3.00
$[0]_8$	240	29.0	3.00
$[90]_8$	199	29.0	3.00
$[90]_8$	170	29.0	3.00
$[90]_8$	185	29.0	3.00
$[90]_8$	158	29.0	3.00
$[0]_4$	141	38.6	0.85
$[0]_4$	143	38.6	0.85
$[0]_4$	205	47.5	0.85
$[0]_4$	211	47.5	0.85

Figure 2 shows a typical response of the original signal measured by the accelerometer and the corresponding filtered response for the first natural frequency (bending mode). Figure 3 displays the original frequency spectrum (Fourier Transform) where the fundamental natural frequency can be identified at 23.23 Hz. This spectrum also shows another resonance around 145 Hz which corresponds to the 1st torsional mode, as later identified via FE analysis.

Figure 4 depicts the post-processing results of the filtered signal (red curve), where the Hilbert transform defined the envelope (black curve), and the exponential curve fitting (green curve) was used to define the damping ratio by logarithm decrement.

Preprints (www.preprints.org) | NOT PEER-REVIEWED | Posted: 15 January 2018 doi:10.20944/preprints201801.0124.v1

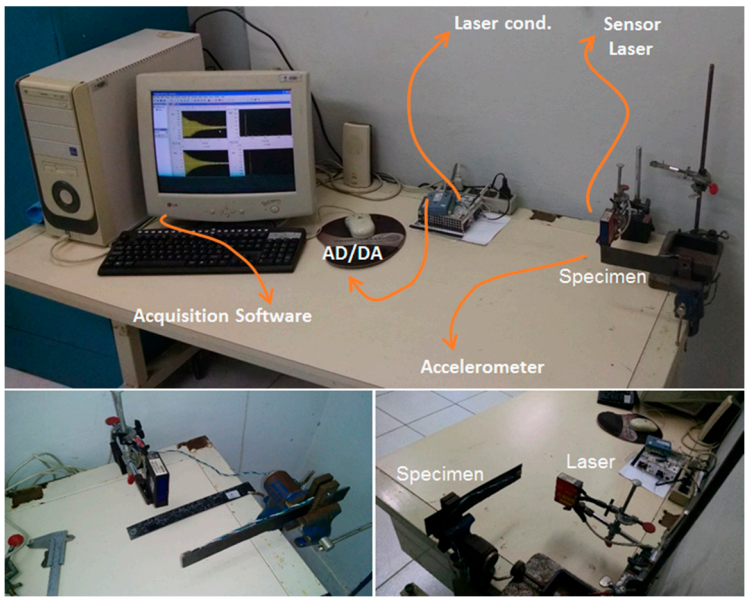

Figure 1. Experimental set-up used for damping ratio evaluation.

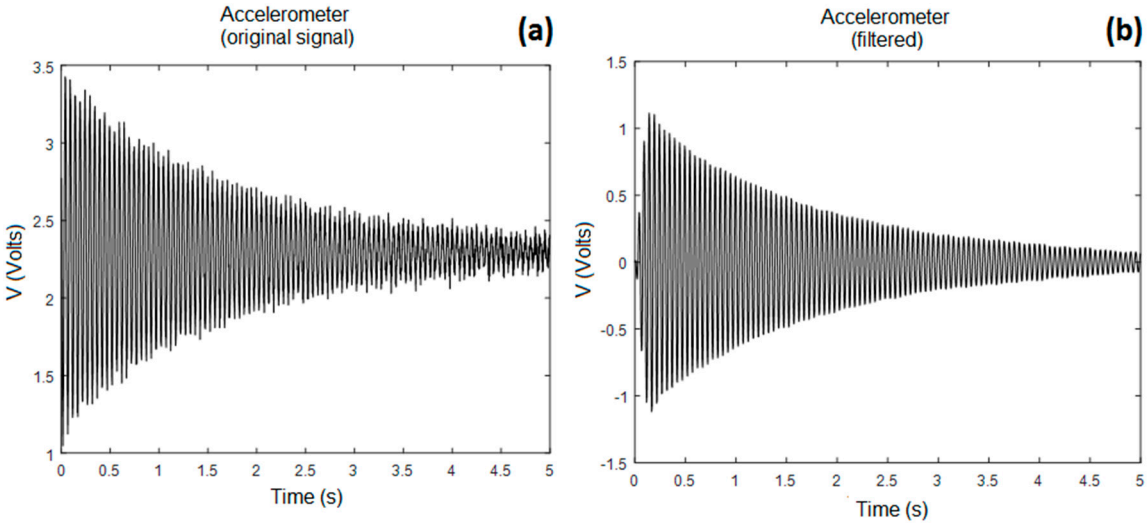

Figure 2. Typical accelerometer output (4th sample, 4th replication): Original (a) and filtered (b) time responses.

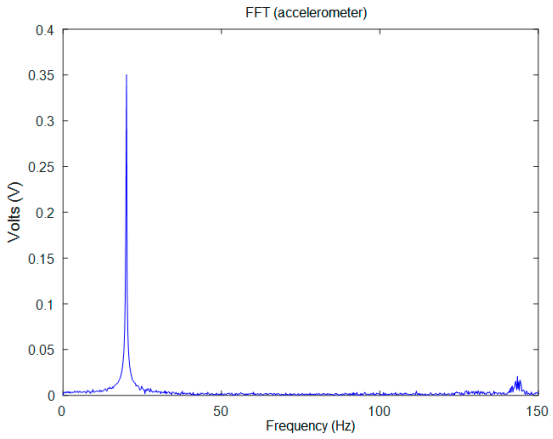

Figure 3. Original free vibration response measured by accelerometer (4th sample, 4th replication).

Preprints (www.preprints.org) | NOT PEER-REVIEWED | Posted: 15 January 2018 doi:10.20944/preprints201801.0124.v1

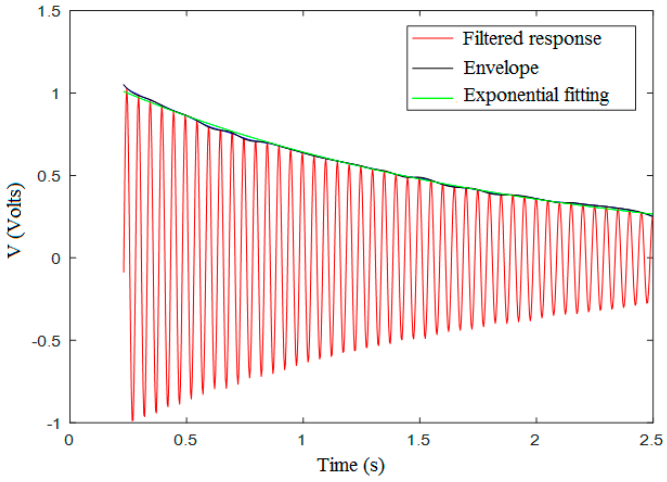

Figure 4. Filtered signal acquired from the accelerometer (red curve), envelope defined by Hilbert transform (black curve) and exponential fitting (green curve) used to define damping ratio.

5. Finite element model

This section is not mandatory, but can be added to the manuscript if the discussion is unusually long or complex.

For the finite element (FE) model herein built, a degenerated 4-node element with bending and torsion capability was adopted. The first-order shear deformation theory (FSDT) for laminated plates (Mindlin plate theory) was followed, where the displacement field is given by:

$$\begin{aligned} u(x,y,z) &= u_0(x,y) + z\theta_x(x,y) \\ v(x,y,z) &= v_0(x,y) + z\theta_y(x,y) \\ w(x,y,z) &= w_0(x,y) \end{aligned} \tag{13}$$

where u, v, and w are the displacement components of the vector field, and θ_i, with $i = x, y$, are the rotations on these axes.

The strain tensor for each layer is obtained from the displacement field using:

$$\begin{Bmatrix} \varepsilon_{xx} \\ \varepsilon_{yy} \\ \gamma_{xy} \\ \gamma_{xz} \\ \gamma_{yz} \end{Bmatrix} = \begin{Bmatrix} \frac{\partial u}{\partial x} \\ \frac{\partial v}{\partial y} \\ \frac{\partial u}{\partial y} + \frac{\partial v}{\partial x} \\ \frac{\partial u}{\partial z} + \frac{\partial w}{\partial x} \\ \frac{\partial v}{\partial z} + \frac{\partial w}{\partial y} \end{Bmatrix} \tag{14}$$

The stiffness matrix is then obtained by usual Gauss integration points throughout each lamina and from the definition of element strain energy. Thus, for instance, the membrane-bending coupling matrix is calculated by:

$$\boldsymbol{K}_{mb}^{(e)} = \sum_{k=1}^{nl} \int_A \boldsymbol{B}_m^T \boldsymbol{D} \boldsymbol{B}_b \; (z_{k+1} - z_k) dA \tag{15}$$

where nl is the number of layers along the total thickness of the laminate, $\boldsymbol{D}$ is the constitutive matrix, already rotated to each layer orientation, $\boldsymbol{B_m}$ and $\boldsymbol{B_b}$ are the matrices of shape function derivatives for the membrane and bending components, respectively, and z_k and z_{k+1} are the top and bottom coordinates of k^{th} layer, respectively.

Superposing the matrices related to each effect, the element matrix can be expressed as:

$$\boldsymbol{K}^{(e)} = \boldsymbol{K}_{mm}^{(e)} + \boldsymbol{K}_{mb}^{(e)} + \boldsymbol{K}_{bm}^{(e)} + \boldsymbol{K}_{bb}^{(e)} + \boldsymbol{K}_{ss}^{(e)} \tag{16}$$

where the indexes mm, mb, bm, bb, and ss stand for membrane, membrane-bending, bending-membrane, bending, and shear effects, respectively. The global matrix is then assembled by superposing each correspondent degree of freedom.

Preprints (www.preprints.org) | NOT PEER-REVIEWED | Posted: 15 January 2018 doi:10.20944/preprints201801.0124.v1

For the time-domain analysis, the equation of motion is commonly given for a general multi-degree of freedom (MDOF) system by:

$$\boldsymbol{M}\{\ddot{\boldsymbol{y}}(t)\} + \boldsymbol{C}\{\dot{\boldsymbol{y}}(t)\} + \boldsymbol{K}\{\boldsymbol{y}(t)\} = \{f(t)\} \quad (17)$$

and the corresponding generalized eigenvector-eigenvalue problem is defined as:

$$(\lambda_i^2\boldsymbol{M} + \lambda_i\boldsymbol{C} + \boldsymbol{K})\{\boldsymbol{\varphi_i}\} = \{0\} \quad (18)$$

where M is the global mass matrix, K is the global stiffness matrix, C is the global damping matrix, λ_i is the ith eigenvalue and $\{\boldsymbol{\varphi_i}\}$ the ith eigenvector (ith column of the $\boldsymbol{\phi}$ generalized eigenvector matrix). So, once the structural matrices are defined and Equation (18) is solved, the damped frequencies can be evaluated by $f_i = Im(\lambda_i)/2\pi$ and the damping ratios by $\zeta_i = -Re(\lambda_i)/(2\pi|\lambda_i|)$. For time domain simulations, the global damping matrix $\boldsymbol{C}$ is selected to be proportional to stiffness and mass, in such a way that it will represent the contribution of the modes with defined damping ratios (nm measured modes): $\boldsymbol{C} = \boldsymbol{M}\sum_{i=1}^{nm}\{\boldsymbol{\varphi_i}\}\zeta_i\{\boldsymbol{\varphi_i}\}^{\boldsymbol{T}}\boldsymbol{M}$.

A 120-element FE mesh was generated for the finite element analysis (see Figure 5). Prior convergence mesh analysis was carried out in order to validate the procedure to obtain representative natural frequencies. The accelerometer mass was added near the free tip of the cantilever to better represent the experimental set-up (also represented in Figure 5).

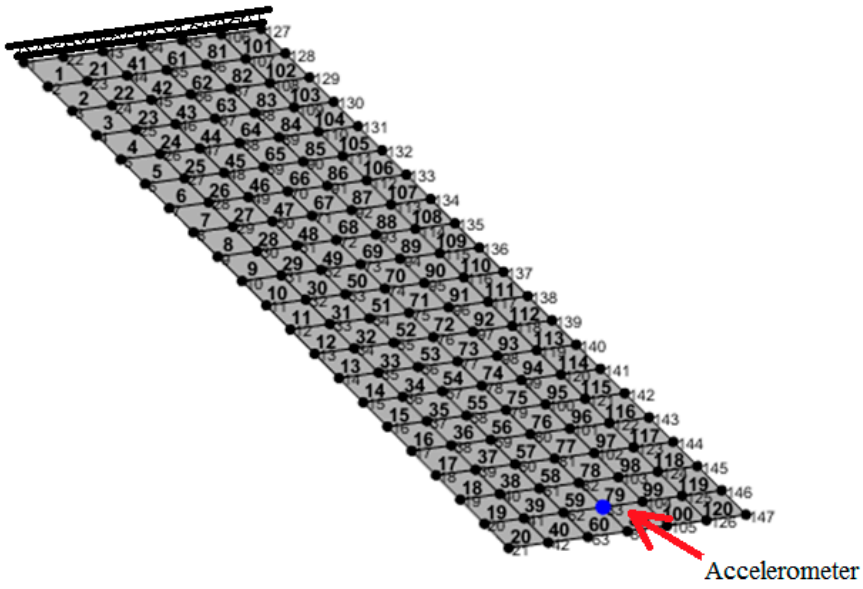

Figure 5. FE mesh illustration with accelerometer position embedded into the FE model.

6. Results and discussion

This section is not mandatory, but may be added if there are patents resulting from the work reported in this manuscript.

The experimental results of natural frequencies and damping ratio for each sample and its replications are shown in Table 3-5. Damping was found to vary according to the number of layers, ply orientation and with specimen length, as expected. The observed damping variability between samples of the same family was considered low, being attributed to changes in overall viscous damping (air drag around oscillating structure), which is more significant for small and simple structures as those herewith tested. It was also observed low variability between replications in the same sample and composite specimen. For instance, in case of specimen [0]4 (Table 3), the samples have standard deviation lower than 0.4% in damping ratio. In the sample specimen, for instance, samples 1 and 2 of Table 3, for an increase in the specimen length of about 3% this resulted in decreasing damping ratio about 37%. Experimental data using accelerometer or the laser transducer resulted in very similar results, so the optical sensor data was preferred, since this acquisition method is non-intrusive.

Preprints (www.preprints.org) | NOT PEER-REVIEWED | Posted: 15 January 2018 doi:10.20944/preprints201801.0124.v1

Table 3. Natural frequencies and damping ratio results for the $[0]_4$ carbon/epoxy specimens.

	Sample 1		Sample 2		Sample 3		Sample 4	
Replication	$f1$	ξ	$f1$	ξ	$f1$	ξ	$f1$	ξ
1	41.66	0.0042	20.23	0.0062	40.45	0.0187	19.63	0.0137
2	41.66	0.0066	20.43	0.0056	40.05	0.0271	19.43	0.0136
3	41.66	0.0043	20.23	0.0066	39.45	0.0162	19.63	0.0141
4	41.86	0.0083	20.23	0.0062	39.25	0.0181	19.43	0.0141
5	41.86	0.0114	20.23	0.0060	39.25	0.0187	19.43	0.0134
6	41.86	0.0117	20.23	0.0057	39.25	0.0190	19.43	0.0131
7	41.86	0.0087	20.03	0.0050	39.05	0.0183	19.43	0.0125
8	41.86	0.0081	20.03	0.0045	39.25	0.0154	19.43	0.0135
9	41.86	0.0097	20.03	0.0045	40.25	0.0140	19.63	0.0129
10	41.86	0.0090	20.03	0.0042	40.25	0.0110	19.43	0.0131
Mean	41.8	0.008	20.2	0.005	39.7	0.018	19.5	0.013
Standard deviation	0.097	0.003	0.135	0.001	0.534	0.004	0.097	0.001
CV	0.002	0.311	0.007	0.153	0.013	0.238	0.005	0.039

Good agreement for modal frequency between experiments and updated numerical model, in the frequency range of the measured data was found, as will be presented in the following, indicating that this updated numerical model can be used to evaluate the dynamic behavior of composite structures.

Table 4. Natural frequencies and damping ratio results for the $[0]_8$ carbon/epoxy specimens.

	Sample 1		Sample 2		Sample 3		Sample 4	
Replication	$f1$	ξ	$f1$	ξ	$f1$	ξ	$f1$	ξ
1	57.65	0.0076	74.49	0.0048	87.30	0.0086	59.47	0.015
2	57.65	0.0094	74.49	0.0048	87.10	0.0054	59.47	0.018
3	57.25	0.0084	74.49	0.0051	87.10	0.0073	59.27	0.022
4	57.25	0.0061	74.49	0.0051	87.10	0.0054	59.27	0.012
5	57.25	0.0066	74.08	0.0054	87.10	0.0064	59.47	0.018
6	57.25	0.0031	74.49	0.0058	87.09	0.0069	59.27	0.021
7	57.65	0.0102	74.49	0.0063	87.10	0.0092	59.27	0.011
8	57.45	0.0112	74.69	0.0053	87.10	0.0069	59.27	0.019
9	57.25	0.0074	74.49	0.0062	87.30	0.0074	59.27	0.012
10	57.65	0.0105	74.49	0.0051	87.10	0.0083	59.27	0.013
Mean	57.4	0.008	74.5	0.005	87.1	0.007	59.3	0.016
Standard deviation	0.199	0.002	0.148	0.001	0.085	0.001	0.097	0.004
CV	0.003	0.299	0.002	0.102	0.001	0.180	0.002	0.249

The results indicate a mean damping ratio (ζ) of 9×10^{-3} (coefficient of variation ca. 15%) for [0]8 sample (Table 4), 4.5×10^{-3} (coefficient of variation ca. 8%) for [90]8 sample (Table 5) and 1.1×10^{-2} (coefficient of variation ca. 18%) for the [0]4 laminate (Table 3). It is worth mentioning that these values lie in the same order of magnitude expected for carbon/epoxy composite damping properties [17]. It can also be said that, the longer the sample, the greater the damping.

Using the results presented in Table 5, for Sample 4 (and 4th replication), for instance, the finite element model was updated with the experimentally identified damping ratio. Numerical mode shapes associated with 1st, 2nd and 4th frequencies are shown in Figure 6 and simulated results for transverse displacement are presented in Figure 7. Analysis of displacement and power spectral density (PSD) of a node at the center of the free tip (node 84) can be used to identify structural modal frequencies. The following values for the first four damped natural frequencies were obtained:

Preprints (www.preprints.org) | NOT PEER-REVIEWED | Posted: 15 January 2018 doi:10.20944/preprints201801.0124.v1

f1=37.41 Hz, f2=261.90 Hz, f3=361.88 Hz and f4=550.51 Hz. One can see that the first natural frequency is very similar to the experimental one indicated in Table 5.

Table 5. Natural frequencies and damping ratio results for the [90]8 carbon/epoxy specimens.

	Sample 1		Sample 2		Sample 3		Sample 4	
Replication	$f1$	ξ	$f1$	ξ	$f1$	ξ	$f1$	ξ
1	23.23	0.0034	33.04	0.0041	26.63	0.0055	37.44	0.0044
2	23.23	0.0048	33.04	0.0047	26.63	0.0061	37.44	0.0045
3	23.23	0.0029	33.04	0.0047	26.63	0.0059	37.44	0.0043
4	23.23	0.0048	33.04	0.0044	26.63	0.0054	37.44	0.0042
5	23.23	0.0053	33.04	0.0045	26.63	0.0051	37.44	0.0045
6	23.23	0.0046	33.04	0.0046	26.63	0.0056	37.44	0.0042
7	23.23	0.0048	33.04	0.0048	26.63	0.0051	37.44	0.0043
8	23.23	0.0048	33.04	0.0039	26.63	0.0057	37.44	0.0044
9	23.23	0.0042	33.04	0.0048	26.63	0.0053	37.44	0.0041
10	23.23	0.0046	33.04	0.0043	26.63	0.0048	37.44	0.0044
Mean	23.2	0.004	33.0	0.004	26.6	0.005	37.4	0.004
Standard deviation	0.000	0.001	0.000	0.000	0.000	0.000	0.000	0.000
CV	0.000	0.163	0.000	0.068	0.000	0.070	0.000	0.031

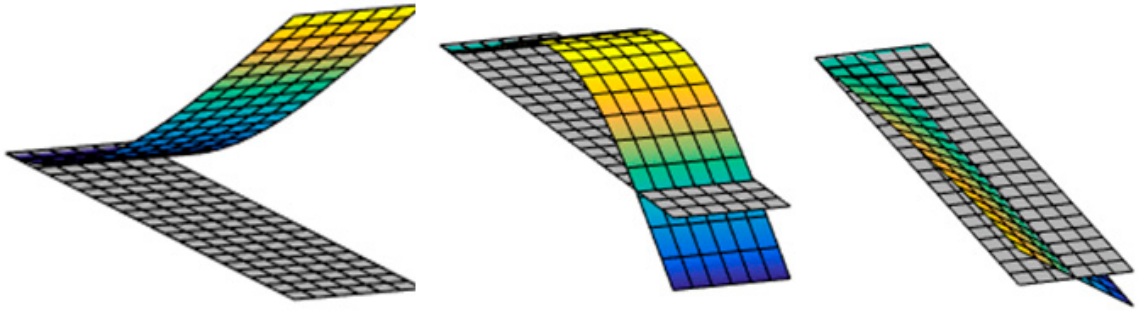

Figure 6. Mode shapes corresponding to 1st (bending), 2nd (bending) and 4th (torsion) modes.

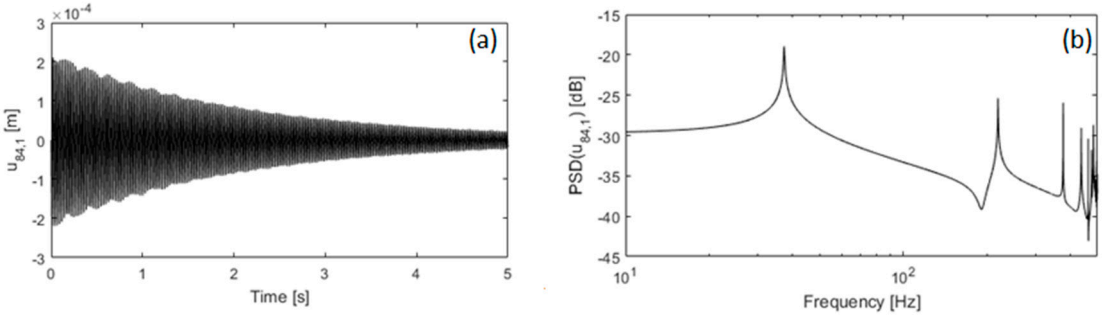

Figure 7. Simulated time response for the transverse displacement of node 84 with damping ratios extracted from experimental data (a) and PSD for the displacement (b).

7. Conclusions

In this study, Hilbert transform was successfully applied for the identification of damping ratio in carbon/epoxy composite laminates. This method was readily implemented and considered a reliable alternative for damping ratio parameter calculations. Stability of this method was verified by the low dispersion of the obtained data (low coefficient of variation), considering the whole set of test repetitions for replicates. Experimental results revealed that damping varied according to the number of layers, ply orientation and specimen length. The damping variability between samples of the same family was attributed to changes in overall viscous damping (air drag around oscillating structures),

 doi:10.20944/preprints201801.0124.v1

276 which is more pronounced in small and simple structures as those samples tested. Also, the proposed
277 method using the Hilbert transform technique allowed quick and systematic evaluation of the
278 variability between samples.
279

280 **Acknowledgements**

281 J.H.S. Almeida Jr. is grateful to CAPES and Alexander von Humboldt-Stiftung (process
282 number 0029/16-5); and H.M. Gomes and S.C. Amico thank CAPES and CNPq.

283

284 **References**

1. Al-Huniti N.; Al-Faqs F,; Zaid O.A. Finite element dynamic analysis of laminated viscoelastic structures, *Appl Compos Mater* **2010**, 17(5), 489-498.
2. Rouf K; Denton NL; French RM. Effect of fabric weaves on the dynamic response of two-dimensional woven fabric composites. *J Mater Sci* **2017**, 52(17), 10581-10591.
3. Berthelot J-M and Sefrani Y. Damping analysis of unidirectional glass and Kevlar fibre composites. *Compos Sci Technol* 64, **2004**, 1261-1278.
4. Hoksbergen JS; Ramulu M; Reinhall Per; Briggs TM. A comparison of the vibration characteristics of carbon fiber reinforced plastic plates with those of magnesium plates. *Appl Compos Mater* **2009**, 16(5), 263-283.
5. Ashworth S; Rongong J; Wilson P; Meredith J. Mechanical and damping properties of resin transfer moulded jute-carbon hybrid composites, *Compos Part B Eng* **2016**, 105, 60-66.
6. Botelho EC; Pardini LC; Rezende MC. Damping behavior of continuous fiber/metal composite materials by the free vibration method. *Compos Part B Eng* **2006**, 37, 255-264.
7. Meftah H; Tamboura S; Fitoussi J; Bendaly H; Tcharkhtchi A. Characterization of a new fully recycled carbon fiber reinforced composite subjected to high strain rate tension. *Appl Compos Mater* **2017**. DOI: 10.1007/s10443-017-9632-6.
8. Lurie S; Minhat M; Tuchkova N; Soliaev J. On remarkable loss amplification mechanism in fiber reinforced laminated composite materials. *Appl Compos Mater* **2014**, 21(1), 179-196.
9. Dubenets VG and Yakovenko OA. Determination of effective damping characteristics of fiber-reinforced viscoelastic composites. *Strength Mater* **2009,** 41(4), 436-443.
10. Wei CY and Kukureka SN. Evaluation of damping and elastic properties of composites and composite structures by resonance technique. *J Mater Sci* **2000**, 35(15), 3785-3792.
11. Fenza A; Monaco E; Amoroso F; Lecce L. Experimental approach in studying temperature effects on composite material structures realized with viscoelastic damping treatments. *J Vib Control* **2014**, 22(6), 358-370.
12. Lavanya K; Krishna PV; Sarcar MMM; Sankar HR. Analysis of the damping characteristics of glass fiber reinforced composite with different orientation and viscoelastic layers. *Int J Conc Mech Civil Eng* **2013**, 1(1), 2357-2360.
13. Harris CM and Piersol AG. Shock and vibration handbook. 5th Edn. McGraw-Hill, 2002, New York.
14. Huang CY and Tsai JL. Characterizing vibration damping response of composite laminates containing silica nanoparticles and rubber particles. *J Compos Mater* **2014**, 49(5), 545-557.
15. Demarie GV and Sabia D. Non-linear damping and frequency identification in a progressively damaged R.C. element. *Exp Mech* **2011**, 51(2), 229-245.
16. Almeida Jr. JHS; Souza SDB; Botelho EC; Amico SC. Carbon fiber-reinforced epoxy filament-wound composite laminates exposed to hygrothermal conditioning. *J Mater Sci* **2016**, 51(9), 4697-4708.
17. Shafi UK; Chi Y-L; Naveed AS; Jang-Kyo K. Vibration damping characteristics of carbon fiber-reinforced composites containing multi-walled carbon nanotubes. *Compos Sci Technol* **2011**, 71(12), 1486–1494.